alone. However, for the jet acting alone, the slot geometry governs the growth of the wake. Given the aforementioned difference noted in the jets issuing from the two ostensibly similar slots, one would expect a complex relation between wake width and bleed coefficient for the cylinders examined. Reference to Fig. 4 in fact shows that for the smaller ($h/D = 0.08$) cylinder, the jet-only wake exceeded the upstream-only wake at $x/D = 5$, whereas for the larger cylinder the upstream-only wake was greater than the jet-only wake. A jet wake of 4.2 behind the smaller cylinder contracted to half that magnitude in a combined flow, whereas the upstream-alone case generated a wake width of 3.1. The contracting effect at higher bleed coefficients was less pronounced for the larger cylinder diameter, but still significant: For $C_q = 0.14$, values dropped from 2.3 for the jet alone to 1.5 for the combined flow. However, most interesting, the results for both cylinders superposed on one another, suggesting that in spite of differences in jet profiles, the bleed coefficient alone is a good predictor of wake width downstream of the jet exit.

Finally vortex shedding activity was observed at a station 10 diameters downstream and 1–2 diameters off the streamwise centerline of each cylinder. The differences in jet geometry had no effect on the persistence of organized shedding, which remained the same as for the upstream-only flow up to $C_q = 0.06$ and then split into a broader range with two identifiable dominant frequencies up to $C_q = 0.11$ before disappearing for higher bleed coefficients. The jet flow had become strong enough to prevent flow from being swept across the wake central axis, as occurs in a vortex formation region. Without that mixing, alternate shedding ceased to exist.

Conclusions

Injection of a jet into the wake produced by an upstream flow around a circular cylinder alters its well-understood dynamics, which now become a function of the geometry of the jet as well as its relative magnitude. Whereas previous investigators who focused solely on the momentumless wake behind a streamlined body found augmentation of the near wake by axisymmetric jet injection, the present paper notes a greater velocity defect in the near wake of a bluff body in the presence of a relatively low jet flow rate. The presence of a jet also decreases the wake width, which depends more on the magnitude of the bleed coefficient than the configuration of the jet. Vortex shedding activity is likewise more a function of bleed coefficient than of jet geometry.

References

[1]Naudascher, E., "Flow in the Wake of Self-Propelled Bodies and Related Sources of Turbulence," *Journal of Fluid Mechanics*, Vol. 22, Pt. 4, 1965, pp. 625–656.

[2]Bradbury, L. J. S., "The Structure of a Self-Preserving Turbulent Plane Jet," *Journal of Fluid Mechanics*, Vol. 23, Pt. 1, 1965, pp. 31–64.

[3]Serviente, A. I., and Patel, V. C., "Wake of a Self-Propelled Body, Part 1: Momentumless Wake," *AIAA Journal*, Vol. 38, No. 4, 2000, pp. 613–619.

[4]Koutmos, P., Mavridis, C., and Papiliou, D., "A Study of Unsteady Wake Flows Past a Two Dimensional Square Cylinder with and Without Planar Jet Injection into the Vortex Formation Region," *Applied Scientific Research*, Vol. 55, No. 3, 1996, pp. 187–210.

[5]Wood, C. J., "Visualization of an Incompressible Wake with Base Bleed," *Journal of Fluid Mechanics*, Vol. 29, Pt. 2, 1967, pp. 259–272.

[6]Zhdanov, V. L., "Effect of Jet Bleed Out of the Base of a Model on the Base Pressure and Frequency Characteristics of Wake Flow," *Journal of Engineering Physics and Thermophysics*, Vol. 71, No. 4, 1998, pp. 627–632.

[7]Duke, R., Shrader, B., and Mo, J., "Effects of a Rear Stagnation Jet on the Wake Behind a Cylinder," *AIAA Journal*, Vol. 31, No. 9, 1993, pp. 1727–1729.

[8]Quinn, W. R., Pollard, A., and Masters, G. F., "Mean Velocity and Static Pressure Distribution in a Three-Dimensional Turbulent Freejet," *AIAA Journal*, Vol. 23, No. 6, 1985, pp. 971–973.

W. J. Devenport
Associate Editor

Rotating Multilayered Cylindrical Shells to Impact Loading

S. W. Gong* and K. Y. Lam†
Institute of High Performance Computing, Singapore 117528, Republic of Singapore

Introduction

IMPACT on multilayered shell structures has been a subject of considerable interest and concern in recent years. Christoforou and Swanson[1] formulated an analytic solution to the problem of simply supported, orthotropic cylindrical shells subjected to impact loading. In their analysis, the deceleration of the impacting mass was used to estimate the impact force. Gong et al.[2] adopted Christoforou and Swanson's approach and undertook analyses of laminated cylindrical shells subjected to impact. In their work, contact deformation was considered, and an analytic function describing it was proposed and incorporated into the analysis. Recently, Gong et al.[3] presented solutions for the problems of functionally graded material (FGM) cylindrical shells subjected to low-velocity impact, and Gong and Lam[4] examined the effects of structural damping on impact response.

None of the preceding studies, however, have dealt with rotating multilayered shells subjected to impact loading. Rotating shells have a wide range of engineering applications, such as in the high-speed centrifugal separator, high-power aircraft jet engine, and the drive shaft of gas turbine, motor, rotor system. With the use of composite material in rotating shell structures, their engineering applications have been extended and improved further.[5] Therefore, a comprehensive study and understanding of transient response of a rotating multilayered shell to impact is essential. The present work addresses this and presents an analytic solution to the problem of a rotating composite shell to impact loading.

Governing Equations

Consider a multilayered cylindrical shell rotating about its symmetrical and horizontal axis at a constant angular speed Ω, as shown in Fig. 1. The shell has a mean radius of R, length of L, and thickness of h. The reference surface of the shell is taken to be at its middle surface, where an orthogonal coordinate system (x, θ, z) is fixed. The displacements of the cylinder in the x, θ, and z directions are defined by u, v, and w, respectively. For the rotating cylindrical shell subjected to a distributed load q_n that is normal to the reference surface, the governing equations of motion for the rotating cylindrical shell can be expressed as

$$\frac{\partial \boldsymbol{N}_x}{\partial x} + \frac{\partial \boldsymbol{N}_{x\theta}}{R\partial\theta} + \tilde{N}_\theta\left(\frac{1}{R^2}\frac{\partial^2 u}{\partial\theta^2} - \frac{1}{R}\frac{\partial w}{\partial x}\right) = \rho h\frac{\partial^2 u}{\partial^2 t} \tag{1}$$

$$\frac{\partial \boldsymbol{N}_{x\theta}}{\partial x} + \frac{\partial \boldsymbol{N}_\theta}{R\partial\theta} + \frac{\partial \boldsymbol{M}_{x\theta}}{R\partial x} + \frac{\partial \boldsymbol{M}_\theta}{R^2\partial\theta} + \frac{\tilde{N}_\theta}{R}\frac{\partial^2 u}{\partial x\partial\theta} = \rho h\left(\frac{\partial^2 v}{\partial^2 t} + 2\Omega\frac{\partial w}{\partial t} - \Omega^2 v\right) \tag{2}$$

Received 23 August 2001; revision received 10 July 2002; accepted for publication 3 September 2002.

*Principal Research Engineer, 1 Science Park Road, Number 01-01 The Capricorn, Singapore Science Park II. Member AIAA.

†Director, 1 Science Park Road, Number 01-01 The Capricorn, Singapore Science Park II.

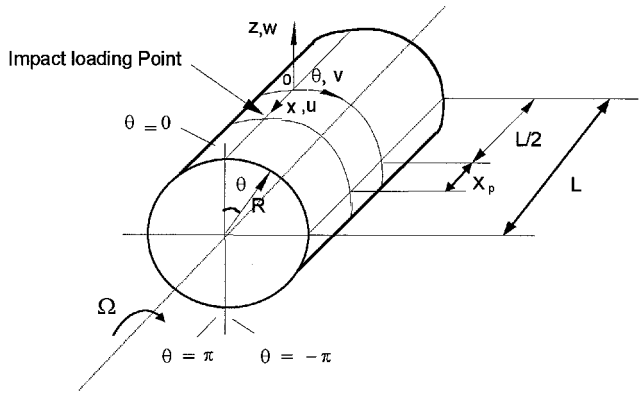

Fig. 1 Rotating cylindrical shell geometry and coordinate system used.

$$\frac{\partial \boldsymbol{M}_x}{\partial x^2} + \frac{2}{R}\frac{\partial^2 \boldsymbol{M}_{x\theta}}{\partial x \partial \theta} + \frac{1}{R^2}\frac{\partial^2 \boldsymbol{M}_\theta}{\partial \theta^2} - \frac{\boldsymbol{N}_\theta}{R} + \frac{\tilde{N}_\theta}{R^2}\left(\frac{\partial^2 w}{\partial \theta^2} - \frac{\partial v}{\partial \theta}\right) = \rho h\left(\frac{\partial^2 w}{\partial^2 t} - 2\Omega\frac{\partial v}{\partial t} - \Omega^2 w\right) - q_n \tag{3}$$

where ρ is the density of the shell. $\tilde{N}_\theta = \rho h \Omega^2 R^2$ is defined as the initial hoop tension due to the centrifugal force effect. $\boldsymbol{N}^T = \{N_x, N_\theta, N_{x\theta}\}$ and $\boldsymbol{M}^T = \{M_x, M_\theta, M_{x\theta}\}$ are force moment vectors respectively. They can be obtained from the constitutive relationship

$$\begin{Bmatrix} \boldsymbol{N} \\ \boldsymbol{M} \end{Bmatrix} = \begin{bmatrix} \boldsymbol{A} & \boldsymbol{B} \\ \boldsymbol{B} & \boldsymbol{D} \end{bmatrix} \begin{Bmatrix} \boldsymbol{e} \\ \boldsymbol{\kappa} \end{Bmatrix} \tag{4}$$

where $\boldsymbol{A} = [A_{ij}]$, $\boldsymbol{B} = [B_{ij}]$, and $\boldsymbol{D} = [D_{ij}]$ are the extensional, coupling, and bending stiffnesses defined, respectively, as

$$(A_{ij}, B_{ij}, D_{ij}) = \sum_{k=1}^{L_k} \int_{z_{k-1}}^{z_k} Q_i^{(k)}(1, z, z^2)\, \mathrm{d}z, \qquad i, j = 1, 2, 6 \tag{5}$$

in which L_k is the number of layers in the shell. Here, $\boldsymbol{e}^T = \{\varepsilon_x^0, \varepsilon_\theta^0, \gamma_{x\theta}^0\}$ and $\boldsymbol{\kappa}^T = \{\kappa_1, \kappa_\theta, \kappa_{x\theta}\}$ are strain and curvature vectors of the reference surface. Both the reference surface strains and the reference surface curvatures can be related to the displacements of the rotating cylindrical shell:

$$\varepsilon_x^0 = \frac{\partial u}{\partial x}, \qquad \varepsilon_\theta^0 = \frac{\partial v}{R\partial \theta} + \frac{w}{R}, \qquad \gamma_{x\theta}^0 = \frac{\partial v}{\partial x} + \frac{\partial u}{R\partial \theta} \tag{6}$$

$$\kappa_x = -\frac{\partial^2 w}{\partial x^2}, \qquad \kappa_\theta = \frac{1}{R^2}\left(-\frac{\partial^2 w}{\partial \theta^2} + \frac{\partial v}{\partial \theta}\right)$$

$$\kappa_{x\theta} = \frac{2}{R}\left(-\frac{\partial^2 w}{\partial x \partial \theta} + \frac{\partial v}{\partial x}\right) \tag{7}$$

When Eq. (4), in conjunction with Eqs. (6) and (7), is substituted into Eqs. (1–3), the equations of motion can be expressed in terms of displacements of the rotating shell:

$$[L_{ij}]\{u, v, w\}^T = \{0, 0, (\rho h \ddot{w} - q_n)\}^T \tag{8}$$

where [ ] and { } represent matices and vectors, respectively, and the differential operators L_{ij} are given in the Appendix. Equation (8) can be used for the dynamic analysis of a rotating cylindrical shell to radial distributed loads with any boundary conditions imposed. In this Note, the simply supported boundary conditions are considered:

$$v(L/2, \theta) = w(L/2, \theta) = \boldsymbol{N}_x(L/2, \theta) = \boldsymbol{M}_x(L/2, \theta) = 0 \tag{9a}$$

$$v[-(L/2), \theta] = w[-(L/2), \theta] = \boldsymbol{N}_x[-(L/2), \theta] = \boldsymbol{M}_x[-(L/2), \theta] = 0 \tag{9b}$$

Solution of Rotating Shell to Impact

For a given distributed dynamic load $q_n(x, \theta, t)$, Navier-type solutions to Eq. (8) that satisfy the boundary conditions (9a) and (9b) can be expressed in the form

$$w(x, \theta, t) = \sum_{m=1}^{\infty}\sum_{n=1}^{\infty} W_{mn}(t) \cos\frac{m\xi^*\pi}{L}(x - x_p)\cos n\theta \tag{10a}$$

$$u(x, \theta, t) = \sum_{m=1}^{\infty}\sum_{n=1}^{\infty} U_{mn}(t) \sin\frac{m\xi^*\pi}{L}(x - x_p)\cos n\theta \tag{10b}$$

$$v(x, \theta, t) = \sum_{m=1}^{\infty}\sum_{n=1}^{\infty} V_{mn}(t) \cos\frac{m\xi^*\pi}{L}(x - x_p)\sin n\theta \tag{10c}$$

In Eqs. (10a–10c), ξ^* is an integer factor defined by

$$\xi^* = [L/(L - 2x_p)]^* \tag{11}$$

where $[f(x_p)]^*$ represents a function that rounds off $f(x_p)$ to the nearest integer. The load $q_n(x, \theta, t)$ is expressed as

$$q_n(x, \theta, t) = \sum_{m=1}^{\infty}\sum_{n=1}^{\infty} Q_{mn}(t) \cos\frac{m\xi^*\pi}{L}(x - x_p)\cos n\theta \tag{12}$$

For a impact loading $F(t)$ at the point $x = x_p$ and $\theta = 0$, $Q_{mn}(t)$ is given by

$$Q_{mn}(t) \approx 2F(t)/L\pi R \tag{13}$$

Substitution of Eqs. (10a–10c) and Eq. (12) into Eq. (8) yields the following equations for the Fourier series coefficients of Eqs. (10a–10c):

$$[\Psi_{ij}]\{U_{mn}, V_{mn}, X_{mn}, \}^T = \{0, 0, [\rho h \ddot{W}_{mn}(t) - Q_{mn}(t)]\}^T \tag{14}$$

where the coefficients Ψ_{ij} are given in the Appendix. From Eq. (14), the Fourier series coefficients yield

$$U_{mn} = K_u W_{mn}, \qquad V_{mn} = K_v W_{mn} \tag{15}$$

where the coefficients K_u, and K_v are given by

$$K_u = \tilde{\Psi}_{31}/\tilde{\Psi}_{33}, \qquad K_v = \tilde{\Psi}_{32}/\tilde{\Psi}_{33} \tag{16}$$

where $\tilde{\psi}_{ij}$ are cofactors of the element Ψ_{ij} in $\det \Psi$.

For a thin cylindrical shell, the strain components have been defined as linear functions of the thickness coordinate z following Love's first approximation theory[6] as

$$\varepsilon_x = \varepsilon_x^0 + z\kappa_x, \qquad \varepsilon_\theta = \varepsilon_\theta^0 + z\kappa_\theta, \qquad \varepsilon_{x\theta} = \gamma_{x\theta}^0 + z\kappa_{x\theta} \tag{17}$$

Substituting Eqs. (10a–10c), in conjunction with Eq. (15), into Eq. (17) yields expressions for strain of the rotating shell:

$$\varepsilon_x(x, \theta, t) = \sum_{m=1}^{\infty}\sum_{n=1}^{\infty}\left[K_u + z\frac{M\xi^*\pi}{L}\right]\frac{M\xi^*\pi}{L} \times W_{mn}(t)\cos\frac{m\xi^*\pi}{L}(x - x_p)\cos n\theta \tag{18a}$$

$$\varepsilon_\theta(x, \theta, t) = \sum_{m=1}^{\infty}\sum_{n=1}^{\infty}\left[K_v + \frac{1}{n} + z\left(\frac{n}{R} + K_v\frac{1}{R}\right)\right]\frac{n}{R} \times W_{mn}(t)\cos\frac{m\xi^*\pi}{L}(x - x_p)\cos n\theta \tag{18b}$$

$$\varepsilon_{x\theta}(x, \theta, t) = \sum_{m=1}^{\infty}\sum_{n=1}^{\infty}\left[-\frac{m\xi^*\pi}{L}K_v - \frac{n}{n}K_u - \frac{2z}{R}\left(\frac{m\xi^*\pi}{L}n + K_v\frac{m\xi^*\pi}{L}\right)\right]\frac{n}{R}W_{mn}(t)\sin\frac{m\xi^*\pi}{L}(x - x_p)\sin n\theta \tag{18c}$$

In this study, we assume that the impact force $F(t)$ is a half-sinusoidal pulse with the peak force F_0 and duration T as follows:

$$F(t) = \begin{cases} F_0 \sin \omega t, & 0 \le t \le T \\ 0, & t \ge T \end{cases} \tag{19}$$

where $T = \pi/\omega$. This force function is substituted into Eq. (14) and integrated to yield

$$W_{mn}(t) = \begin{cases} \dfrac{4F_0}{\omega_{mn} m_1 \left(\omega^2 - \omega_{mn}^2\right)} (\omega \sin \omega_{mn} t - \omega_{mn} \sin \omega_1 t), & 0 < t < T \\ \dfrac{4F_0}{\omega_{mn} m_1 \left(\omega^2 - \omega_{mn}^2\right)} [\omega \sin \omega_{mn} t + \omega \sin \omega_{mn} (t - T)], & t > T \end{cases} \tag{20}$$

When Eqs. (20), (15), (10a–10c), and (18a–18c) are combined, the displacement and strains in the impacted rotating shell can be evaluated.

Results

The present solution facilitates the studies of the transient response of rotating composite shells to impact loading. Consider a $[0_8]$ glass/epoxy cylindrical shell with a mean radius of 0.108 m, a length of 0.28 m, and a thickness of 2.3 mm, rotating with speed of Ω. Its material properties are the same for all of the layers: $E_1 = 14.51$ GPa, $E_2 = 5.36$ GPa, $G_{12} = 2.51$ GPa, $\nu_{12} = 0.231$, and $\rho = 1901.5$ kg/m^2. The numerical calculations are carried out for the transient response of the rotating shell to impact loading.

In this study, the ratio of the impact force parameter ω to the rotating speed of shell Ω is denoted by λ, where

$$\lambda = \omega / \Omega \tag{21}$$

Large values of λ correspond to a shell with lower rotating speed subjected to more impulsive impact, whereas small values of λ denote a shell with higher rotating speed subjected to more "static" impact. The effect of λ is examined for the case where the peak value of impact loading is 150 N. The impact loading is exerted at the central point $(x_p = 0, \theta = 0)$, The ratio λ is varied while the other parameters for the geometry and material properties of the rotating shell are kept constant.

Figure 2 shows the variations of the radial displacement at the central point $(x = 0, \theta = 0)$ with time for different ratios: $\lambda = 30$, 50, and 100. The curves show that the maximum displacements occur after $t = 2$ ms with the maximum value reduced as the ratio λ decreases. Hoop strain distributions along the inner surface of the rotating shell were calculated using Eq. (21). Figure 3 shows the hoop strain distributions along the curve $x = 0$ and $-\pi \le \theta \le \pi$ of the rotating shell at two instants of time during loading. At each instant, three distributions are plotted corresponding to different ratios of λ.

Figure 3 shows that the strain distributions exhibit a similar profile for all of the ratios of λ. The tensile strains initiate at the loading point $x = 0$ and $\theta = 0$. The strains decay rapidly with distance from the impact loading point. As time increases, tensile strains around the impact loading point increase in magnitude. Figure 3 also shows that the strains decrease as the ratio λ reduces. These results indicate that the ratio λ has a significant effect on the transient response of the rotating shell.

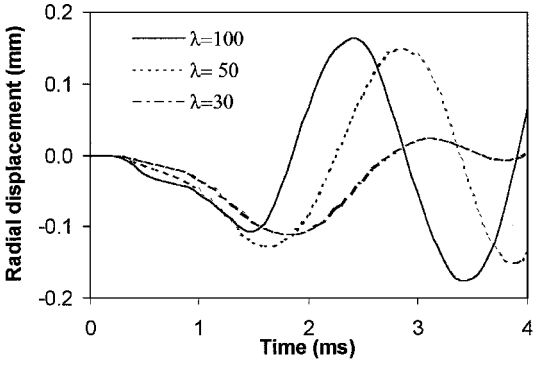

Fig. 2 Variations of the radial displacement with time for ratios λ ranging from 30 to 100.

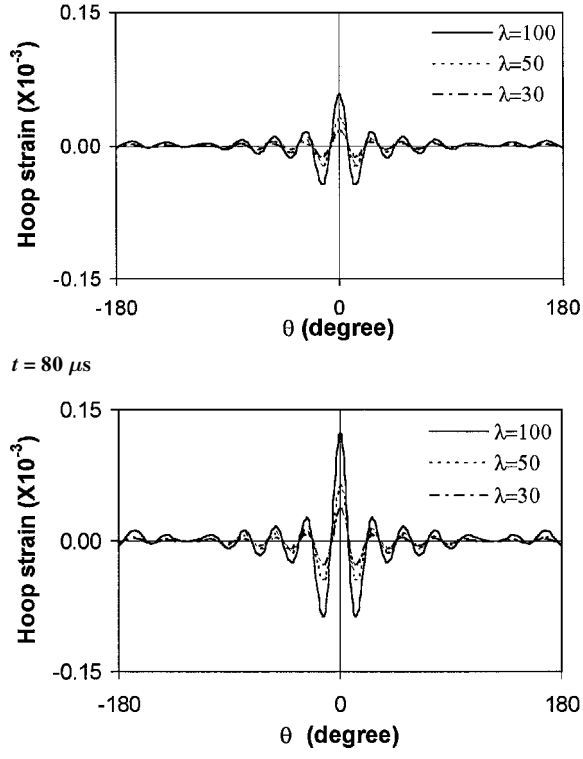

Fig. 3 Hoop strain distribution along θ axis on the inner surface of the cylindrical shell from 80 to 160 μs after impact; $x = 0$.

Conclusions

An analytic solution has been presented for the problem of a rotating composite shell to impact loading that facilitates the study of the transient response of a rotating cylindrical multilayer shell to impact loading. The results show that the ratio of the impact force parameter ω to the rotating speed of shell Ω has a significant effect on the transient response of the rotating shell.

Appendix: Differential Operators and Coefficients

Differential operators $\boldsymbol{L}_{ij}$ in Eq. (8) are

$$L_{11} = A_{11} \frac{\partial^2}{\partial x^2} + A_{66} \frac{\partial^2}{R^2 \partial \theta^2} + \rho h \Omega^2 \frac{\partial^2}{\partial \theta^2} - \rho h \frac{\mathrm{d}^2}{\mathrm{d}t^2}$$

$$L_{12} = \left(A_{12} + A_{66} + \frac{B_{12} + 2B_{66}}{R} \right) \frac{\partial^2}{R \partial x \partial \theta}$$

$$L_{13} = -B_{11} \frac{\partial^3}{\partial x^3} - (B_{12} + 2B_{66}) \frac{\partial^3}{R^2 \partial x \partial \theta^2} + \left(\frac{A_{12}}{R} \right) \frac{\partial}{\partial x} - \rho h \Omega^2 R \frac{\partial}{\partial x}$$

$$L_{21} = \left(A_{12} + A_{66} + \frac{B_{12} + 2B_{66}}{R} \right) \frac{\partial^2}{R \partial x \partial \theta} + \rho h \Omega^2 R \frac{\partial^2}{\partial x \partial \theta}$$

$$L_{22} = \left(A_{66} + \frac{3B_{66}}{R} + \frac{2D_{66}}{R^2} \right) \frac{\partial^2}{\partial x^2} + \left(A_{22} + \frac{2B_{22}}{R} + \frac{D_{22}}{R^2} \right) \frac{\partial^2}{R^2 \partial \theta^2} + \rho h \Omega^2 - \rho h \frac{\mathrm{d}^2}{\mathrm{d}t^2}$$

$$L_{23} = -\left(B_{12} + 2B_{66} + \frac{D_{12} + 2D_{66}}{R}\right)\frac{\partial^3}{R\partial x^2 \partial\theta} + \left(\frac{A_{22}}{R} + \frac{B_{22}}{R^2}\right)\frac{\partial}{R\partial\theta} - \left(B_{22} + \frac{D_{22}}{R}\right)\frac{\partial^3}{R^3\partial\theta^3} - 2\rho h\Omega\frac{\partial}{\partial t}$$

$$L_{31} = B_{11}\frac{\partial^3}{\partial x^3} + (B_{12} + 2B_{66})\frac{\partial^3}{R^2\partial x\partial\theta^2} - \left(\frac{A_{12}}{R}\right)\frac{\partial}{\partial x}$$

$$L_{32} = \left(B_{12} + 2B_{66} + \frac{D_{12} + 4D_{66}}{R}\right)\frac{\partial^3}{R\partial x^2\partial\theta} - \left(\frac{A_{22}}{R} + \frac{B_{22}}{R^2}\right) \times \frac{\partial}{R\partial\theta} + \left(B_{22} + \frac{D_{22}}{R}\right)\frac{\partial^3}{R^3\partial\theta^3} - \rho h\Omega^2\frac{\partial}{\partial\theta} + 2\rho h\Omega\frac{\partial}{\partial t}$$

$$L_{33} = -D_{11}\frac{\partial^4}{\partial x^4} - 2(D_{12} + 2D_{66})\frac{\partial^4}{R^2\partial x^2\partial\theta^2} - D_{22}\frac{\partial^4}{R^4\partial\theta^4} + 2\frac{B_{12}}{R}\frac{\partial^2}{\partial x^2} + 2\frac{B_{22}}{R^3}\frac{\partial^2}{\partial\theta^2} - \frac{A_{22}}{R^2} + \rho h\Omega^2\frac{\partial^2}{\partial\theta^2} + \rho h\Omega^2 - \rho h\frac{\mathrm{d}^2}{\mathrm{d}t^2} \tag{A1}$$

The coefficients ψ_{ij} in Eq. (14) are

$$\psi_{11} = -A_{11}\boldsymbol{M}^2 - A_{66}\boldsymbol{N}^2 - \rho h\Omega^2 R^2\boldsymbol{N}^2 - \rho h\frac{\partial^2 u}{\partial t^2}$$

$$\psi_{12} = -\left(A_{12} + A_{66} + \frac{B_{12} + 2B_{66}}{R}\right)\boldsymbol{MN}$$

$$\psi_{13} = -B_{11}\boldsymbol{M}^3 - (B_{12} + 2B_{66})\boldsymbol{MN}^2 - \frac{A_{12}}{R}\boldsymbol{M} + \rho h\Omega^2 R\boldsymbol{M}$$

$$\psi_{21} = -\left(A_{12} + A_{66} + \frac{B_{12} + B_{66}}{R}\right)\boldsymbol{MN} - \rho h\Omega^2 R^2\boldsymbol{MN}$$

$$\psi_{22} = -\left(A_{66} + \frac{3B_{66}}{R} + \frac{2D_{66}}{R^2}\right)M^2 - \left(A_{22} + \frac{2B_{22}}{R} + \frac{D_{22}}{R^2}\right)N^2 + \rho h\Omega^2 - \rho h\frac{\mathrm{d}^2 v}{\mathrm{d}t^2}$$

$$\psi_{23} = -\left(B_{22} + \frac{D_{22}}{R}\right)N^3 - \left(B_{12} + 2B_{66} + \frac{D_{12} + 2D_{66}}{R}\right)M^2 N - \left(\frac{A_{22}}{R} + \frac{B_{22}}{R^2}\right)N - 2\rho h\Omega\frac{\partial w}{\partial t}$$

$$\psi_{31} = -B_{11}M^3 - (B_{12} + 2B_{66})\boldsymbol{MN}^2 - \frac{A_{12}}{R}\boldsymbol{M}$$

$$\psi_{32} = -\left(B_{22} + \frac{D_{22}}{R}\right)\boldsymbol{N}^3 - \left(B_{12} + 2B_{66} + \frac{D_{12} + 4D_{66}}{R}\right)\boldsymbol{M}^2\boldsymbol{N} - \left(\frac{A_{22}}{R} + \frac{B_{22}}{R^2}\right)N - \rho h\Omega^2 RN + 2\rho h\Omega\frac{\partial v}{\partial t}$$

$$\psi_{33} = -D_{11}\boldsymbol{M}^2 - 2(D_{12} + 2D_{66})\boldsymbol{M}^2\boldsymbol{N}^2 - D_{22}\boldsymbol{N}^4 - 2\frac{B_{12}}{R}M^2 - 2\frac{B_{22}}{R}N^2 - \frac{A_{22}}{R^2} - \rho h\Omega^2 R^2 N^2 + \rho h\Omega^2 - \rho h\frac{\mathrm{d}^2 w}{\mathrm{d}t^2} \tag{A2}$$

where $\boldsymbol{M} = m\xi^*\pi/L$ and $\boldsymbol{N} = n/R$.

References

[1]Christoforou, A. P., and Swanson, S. R., "Analysis of Simply-Supported Orthotropic Cylindrical Shells Subject to Lateral Impact Loads," *Journal of Applied Mechanics*, Vol. 57, June 1990, pp. 376–382.

[2]Gong, S. W., Shim, V. P. W., and Toh, S. L., "Central and Noncentral Normal Impact on Orthotropic Composite Cylindrical Shells," *AIAA Journal*, Vol. 34, No. 8, 1996, pp. 1619–1626.

[3]Gong, S. W., Lam, K. Y., and Reddy, J. N., "The Elastic Response of Functionally Graded Cylindrical Shells to Low Velocity Impact," *International Journal of Impact Engineering*, Vol. 22, No. 4, 1999, pp. 397–417.

[4]Gong, S. W., and Lam, K. Y., "Effects of Structural Damping and Stiffness on Impact Response of Layered Structure," *AIAA Journal*, Vol. 38, No. 9, 2000, pp. 1730–1735.

[5]Li, H., and Lam, K. Y., "Orthotropic Influence on Frequency Characteristics of a Rotating Composite Laminated Conical Shell by the Generalized Differential Quadrature Method," *International Journal of Solids and Structures*, Vol. 38, Nos. 22–23, 2001, pp. 3995–4015.

[6]Love, A. E. H., *A Treatise on the Mathematical Theory of Elasticity*, 4th ed., Cambridge Univ. Press, Cambridge, England, U.K., 1952.

K. N. Shivakumar
Associate Editor